BBA - Proteins and Proteomics 1867 (2019) 701–709

Contents lists available at ScienceDirect

BBA - Proteins and Proteomics

journal homepage: www.elsevier.com/locate/bbapap

α-Synuclein aggregation at low concentrations

Kseniia Afitska[a,b,*], Anna Fucikova[c], Volodymyr V. Shvadchak[a], Dmytro A. Yushchenko[a,d,*]

[a] Institute of Organic Chemistry and Biochemistry, Academy of Sciences of the Czech Republic, Flemingovo namesti 2, Prague 16610, Czech Republic
[b] Department of Biochemistry, Faculty of Science, Charles University, Albertov 6, Prague 12843, Czech Republic
[c] Department of Chemical Physics & Optics, Faculty of Mathematics & Physics, Charles University, Ke Karlovu 3, Prague 12116, Czech Republic
[d] Miltenyi Biotec GmbH, Friedrich-Ebert-Straße 68, Bergisch Gladbach 51429, Germany

ARTICLE INFO

Keywords:
Amyloid fibrils
Kinetics
Fibril disaggregation
Critical concentration
Intermediates
Kd

ABSTRACT

Background: Aggregation of the neuronal protein α-synuclein into amyloid fibrils is a hallmark of Parkinson's disease. The propensity of α-synuclein to aggregate increases with the protein concentration. For the development of efficient inhibitors of α-synuclein aggregation, it is important to know the critical concentration of aggregation (the concentration of monomeric protein, below which the protein does not aggregate).
Methods: We performed in vitro aggregation studies of α-synuclein at low concentrations (0.11–20 μM). Aggregation kinetics was measured by ThT fluorescence. Obtained aggregates were characterized using CD-spectroscopy, fluorescent spectroscopy, dynamic light scattering and AFM imaging.
Results: Monomeric α-synuclein at concentrations 0.45 μM and above was able to bind to fibril ends resulting in fibril growth. At the protein concentrations below 0.4 μM, monomers did not fibrillize, and fibrils disaggregated. In the absence of seeds, fibrils were formed only at monomer concentrations higher than 10 μM. At low micromolar concentrations, we observed formation of prefibrillar amyloid aggregates, which are able to induce fibril formation in α-synuclein solutions of high concentrations.
Conclusions: The critical concentration of α-synuclein fibril growth is ~0.4 μM. Prefibrillar amyloid aggregates appear at concentrations between 0.45 and 3 μM and are an intermediate state between monomers and fibrils. Although morphologically different from fibrils, prefibrillar aggregates have similar properties to those of fibrils.
General significance: We determined the critical concentration of α-synuclein fibril growth. We showed that fibrils can grow at much lower monomer concentrations than that required for de novo fibril formation. We characterized a prefibrillar intermediate species formed upon aggregation of α-synuclein at low micromolar concentration.

1. Introduction

α-synuclein (AS) is an intrinsically disordered protein expressed in neurons. Its physiological function is believed to be related to synaptic vesicle homeostasis and trafficking [1,2]. During the course of Parkinson's disease, AS in dopaminergic neurons misfolds and forms fibrils that later assemble into the pathological inclusions called Lewy bodies. This makes understanding and prevention of AS fibrillization an important task for the development of therapies against this incurable disease.

In vitro monomeric AS spontaneously aggregates forming amyloid fibrils, which appear only after a certain period of incubation (Fig. S1). This period is called the 'lag phase' and may last up to several days. Lag phase terminates with the formation of short initial fibrils. These fibrils further elongate via binding of monomeric protein to the fibril ends, which serve as fibril growth centres. Long fibrils can break providing new free fibril ends [3]. This makes the aggregation autocatalytic and very fast after the first fibrils appear.

The processes that precede formation of fibrils are not yet understood due to the transient nature of the appearing species. There is a hypothesis that an intermediate oligomeric state exists in between the monomeric and fibrillar states of AS [1,4–7]. These oligomers are believed to be a very diverse group of metastable complexes of monomeric subunits. They differ by number of monomers, morphology, structure and seeding capability, depending on conditions of formation and isolation [8]. AS oligomers have been reported to be cytotoxic. This cytotoxicity may be due to the disruption of membranes [5,9–12]. Meanwhile, the interplay between monomers, oligomers and fibrils is

Abbreviations: AS, α-synuclein; AFM, atomic force microscopy; DLS, dynamic light scattering; ThT, Thioflavin T

* Corresponding author at: Institute of Organic Chemistry and Biochemistry Academy of Sciences of the Czech Republic, Flemingovo namesti 2, Prague 16610, Czech Republic
E-mail address: yushchenko@uochb.cas.cz (D.A. Yushchenko).

https://doi.org/10.1016/j.bbapap.2019.05.003
Received 15 January 2019; Received in revised form 8 May 2019; Accepted 10 May 2019
Available online 13 May 2019

not yet well studied, and it is unclear whether oligomers are intermediates of fibril formation.

In most *in vitro* studies, aggregation of AS is investigated at concentrations above 50 μM. Meanwhile, concentration of AS in the synapse is ≈22 μM [13] and is presumably lower in the neuron body. In this regard, it is important to know the lowest (critical) concentration at which AS is still able to form fibrils and below which fibrils undergo disaggregation. Finding this critical concentration of fibrillization is essential not only for the general understanding of AS biology, but also for the development of AS fibrillization inhibitors.

There have been several attempts to determine the critical concentration of AS fibrillization. The minimal concentration at which monomeric AS can form fibrils was found to be in the range 15–28 μM [14,15]. In the presence of arachidonic acid or anionic detergents [16], lipid bilayers [17] or upon ultrasonication [18], fibrillization can also occur within 1–4 μM concentration range. However, in most of these works, only fibril formation was detected, while the kinetics of fibril growth was not studied. In addition, formation of amorphous aggregates on a mica surface has been shown for 10 and 100 nM AS-140C [19], and the formation of branched aggregates on negatively charged supported lipid bilayers or glass surfaces has been shown for 1 nM AS [20]. Nevertheless, these aggregates did not resemble fibrils. This observation raises the question whether aggregates obtained at high concentrations have the same morphology as aggregates obtained at low (close to critical) concentrations [21].

In the present study, we endeavoured to find the critical concentration of AS fibril growth (the lowest concentration of monomeric AS capable of binding to the fibril end) separately from the critical concentration of fibril formation (the lowest concentration of monomeric AS at which new fibrils can form). With this aim, we performed aggregation of AS at low concentrations in the presence and absence of small amount of very short fibrils (seeds). We also studied the structural properties of the obtained aggregates.

2. Materials and methods

2.1. Protein expression

Protein expression and purification was performed as described in our previous work [22]. Shortly, AS was expressed in E.coli, purified by ion-exchange FPLC and stored in 10 mM Tris-HCl, pH 7.4 buffer at ~200 μM protein concentration at −20 °C. Protein stock was centrifuged for 35 min at 13500*g* before each experiment to remove any possible aggregates formed during preparation steps; concentration of protein was measured after the centrifugation by UV absorption using $\varepsilon_{275} = 6000\ M^{-1}\ cm^{-1}$. For the experiments we used three different batches of AS (expressed and purified separately, with difference in several months), and obtained results were reproducible.

2.2. Kinetic measurements

Aggregation experiments were performed using a Tecan Spark plate reader and monitored by Thioflavin T (ThT) fluorescence. All experiments were performed at 37 °C. ThT fluorescence was measured every 300 s, with 5 s shaking (double orbital, 3 mm amplitude) between measurements. Excitation wavelength was 441 nm (slit 5 nm), emission 480 nm (slit 20 nm, gain 90) and fluorescence signal was collected from the bottom. Experiments were performed in 384-well plates (transparent bottom, “Nunc”, Thermo Fisher Scientific) unless stated otherwise. The plates were sealed with film (“Viewseal”, Greiner Bio One) to avoid evaporation. Sample volume was 50 μl per well, that allowed efficient mixing of the sample during shaking. The final solution used for aggregation experiments contained 6 mM pH 7.2 Na-PO_4 buffer, 140 mM NaCl, 10 mM NaN_3, 1 mM EDTA (to remove divalent ions bound to AS), and 5 μM ThT. Protein concentrations for seeded and non-seeded aggregations were 0.11–20 μM, prepared by serial dilutions from 20 and 15 μM solutions; each protein concentration was represented by 3, 6 or 8 repeats depending on the experiment.

2.2.1. Seeded aggregation

Seeds (short fibrils used as fibrillization centres) were prepared by mixing several aggregated AS samples that reached the plateau of ThT fluorescence. The obtained solution was sonicated in an Eppendorf tube for 15 min in a low power bath sonicator (Sonorex Digitec DT 100) to break fibrils into relatively short fragments of ~50–70 nm, corresponding to 100–140 protein units (see section S-2 for more details). Sonication and seeds addition to the reaction mixture were performed directly before the start of measurements (not longer than 1 h from the sonication to the beginning of the measurements, since seeds gradually lose their activity with time). Eppendorf tubes with protein solutions of different concentrations were prepared, and seeds were added simultaneously to the different tubes. Samples were then mixed, pipetted into a plate and fluorescence intensity was measured for ~72 h. Final concentration of seeds in solution was 50 or 200 nM unless stated otherwise. The experiment was performed 4 times with reproducible results.

After ~72 h of aggregation, aliquots of aggregated samples (aggregation in the presence of 50 nM seeds) were taken for AFM investigation (data shown in the section 3.3).

Calculation of fibril growth rate. ThT signal is linearly proportional to fibril concentration (Fig. S5 A, B). Therefore, the fibril growth rate was calculated from the slope of the initial linear part of a kinetic curve according to equation

$$Rate = \frac{I_{t1} - I_{t2}}{t1 - t2},$$

where I_{t1} and I_{t2} are fluorescence intensities at time points t_1 and t_2. t_1 and t_2 were selected individually for each sample to fully cover the range where the curve is linear. t_1 was appr. 300–1400 s (avoiding the region where fluorescent signal was not stable yet), and t_2 was in the range between 2400 s for fast growing samples and 7000–40,000 s for slowly growing samples. This equation was used for calculating fibril growth rate in all the experiments.

Calculation of K_d. We calculated fibril growth rate as described before, and plotted it as a function of monomer concentration. Obtained data were fitted by equation

$$Rate = const\,(C_{monomer} - K_d)$$

using Origin software. These data are presented at Fig. 1B. Final K_d value was obtained as average from 3 independent calculations (data from 3 independent experiments).

ΔG of the reaction of monomer binding to fibril end was calculated as

$$\Delta G = -RTln(K)$$

$$\Delta G = 2.48\ kJ/mol \cdot \ln(4 \times 10^{-7}) = -36.5\ kJ \cdot mol,$$

where 4×10^{-7} is K_d divided by standard concentration of 1 mol/l.

2.2.2. Disaggregation of seeds

Seeds prepared as described above (section 2.2.1) were pipetted into the plate at concentrations of 2, 1, 0.8, 0.6, 0.4, 0.2, 0.1 and 0.05 μM (8 repeats of 50 μl for each sample). Equal volumes of freshly prepared monomeric AS (50 μl of 40 μM solution) were added to 4 wells of each sample (control group) and fluorescence intensity was measured in plate reader for 24 h. After that monomeric AS was added to the remaining 4 repeats (measured group) of each sample, and fluorescence intensity was further measured for ~62 h.

The value of fluorescence intensity of the incubated seeds was taken at 24 h (before monomer addition), and baseline signal of buffer was subtracted. Fluorescence intensity is proportional to the fibril concentration. Therefore, the fraction of intact seeds was calculated in a

following way: the average fluorescence intensity of 4 repeats for each sample was divided by the initial seeds concentration in the sample.

Fibril elongation rate was calculated from the initial linear part of the kinetic curve as described above. As fibril elongation rate depends on the amount and quality of seeds, we calculated relative seeding efficiency of the incubated seeds as the ratio of the fibril elongation rate of the samples with incubated seeds to the fibril elongation rate of samples with fresh seeds, multiplied by 100%.

2.2.3. Non-seeded aggregation

Aggregation of 0.11–20 μM AS (8 repeats for each concentration) was performed in the absence of seeds (Fig. S8).

2.3. AFM imaging

Protein samples were taken from aggregation experiments (for more details see sections 2.2.1 and 2.2.3). Eight microliters of fibrillized protein in sample buffer was resuspended in 100 μl of deionized water. Immediately after that aliquots of 2 μl were placed on the surface of a fresh mica disc and air-dried. The freshly prepared sample was completely characterized by AFM < 2 h after drop casting. AFM images were collected with a JPK Nanowizard 3 combined with IX73 Olympus microscope. The measurements of fibril height were done in a semi-contact mode (AC Mode), and a cantilever ACTA from APPnano was used. At least six different regions of each sample (aggregates on mica) were examined in order to verify that the observed structures demonstrate similar properties throughout the whole sample. Image resolution was 512 × 512 pixels for both 10 × 10 μm and 2 × 2 μM images.

2.4. CD spectroscopy

2.4.1. Sample preparation

Aggregation of 1.25 and 2.5 μM AS samples (triplicates of 1.5 ml) was performed in the thermoshaker at +37 °C, 220 rpm. The aggregation buffer composition was the same as described above, with the exception that no ThT was added as it would interfere with measurements. The reaction was started by adding 50 nM seeds (30 min sonication, no ThT). Aliquots of 200 μl were taken 48 h after start of aggregation. Before measurement aliquots were sonicated for 10 min in a low power bath sonicator (SONOREX DIGITEC DT 100) to ensure uniform distribution of aggregates in solution. Also, we recorded spectra of seeds used for initiation of aggregation, of monomer, and of 1.25 and 2.5 μM fibrils (prepared from completely fibrillized 50 μM protein). All the spectra were corrected to the background spectra of the buffer.

2.4.2. Circular dichroism (CD) spectra

Circular dichroism (CD) spectra were recorded with a JASCO-J210 spectropolarimeter using a 1 mm pathlength cuvette at room temperature, scanning from 210 to 250 nm with a step size of 0.2 nm and a scanning speed of 20 nm/min. The signal/noise ratio was improved by taking and averaging 7 scans. All spectra were corrected by subtracting the background spectrum of the buffer. Values obtained by averaging signal from 217 to 220 nm were taken as proportional to β-sheet content. As we aimed to verify whether signal of prefibrillar amyloid aggregates was not a combination of signals of monomeric protein and seeds, we did not calculate the absolute value of mean residue ellipticity, but instead compared CD signals.

2.5. Aggregation sensed by environmentally sensitive dyes

2.5.1. Protein labelling

A cysteine mutant of AS (AS-18C) was expressed as described above and stored in 10 mM Tris-HCl, pH 7.4 buffer at ~200 μM protein concentration. Protein labelling with maleimide derivatives of solvatochromic dyes FPM, XXL, 6FM and 7AFM was performed as previously reported [23]. Labelled proteins were centrifuged at 13500 *g* for 35 min before use. After centrifugation the concentrations of labelled proteins were measured using absorbance of the correspondent labels [24]: $\varepsilon = 37{,}000\ M^{-1}\,cm^{-1}$ for XXL- and $\varepsilon = 30{,}000\ M^{-1}\,cm^{-1}$ for FPM-, 6FM-, and 7AFM-derivatives (at the absorbance maxima in aqueous 10 mM Tris-HCl buffer, pH 7.4).

2.5.2. Aggregation reaction

We performed aggregation of 50, 20 and 2 μM AS in the presence of 400 nM labelled AS. As ThT fluorescence would interfere with the fluorescence of environmentally sensitive dyes, we used ThT-free aggregation buffer. Seeds concentration was 1 μM (for 50 μM protein) or 200 nM (for 20 and 2 μM protein). Seeds contained no ThT or labelled protein. Aggregation was performed in a 96-well plate (transparent bottom, "Nunc", Thermo Fisher Scientific) sealed with film ("Viewseal", Greiner Bio One) to avoid evaporation. Each sample was prepared in a triplicate with final volume 250 μl per well. The plate was placed in the plate reader to maintain conditions identical to other aggregation experiments (37 °C, 5 s shaking out of 300 s cycle). After 42 h of aggregation, all three repeats of each sample were mixed, and 450 μl of aggregation solution were used for recording the emission spectra. As a control, spectra of 400 nM monomeric labelled protein were recorded.

2.5.3. Fluorescence measurements

Emission spectra were recorded on a Fluoromax-4 spectrofluorometer (Horiba Scientific) using a quartz cuvette with a 0.2 cm pathlength. All spectra were corrected for Raman scattering by subtraction of the corresponding buffer spectrum. Measurements were performed at room temperature. Excitation wavelength, excitation and emission slits were chosen to give the best resolution for each dye and are listed below; integration time was 0.2 s per point.

6FM:Excitation wavelength = 410 nm; slits 2/2 nm.

7AFM:Excitation wavelength = 410 nm; slits 3/3 nm.

XXL: Excitation wavelength = 370 nm; slits 2/3 nm.

FPM: Excitation wavelength = 390 nm; slits 2/3 nm.

Simulated spectra for all dyes were obtained by linear combination of spectra of labelled protein in monomeric and fibrillized form in the ratio selected to best fit the experimental data.

$$Simulated\ spectrum = a \times spectrum_{fibril} + (1 - a) \times spectrum_{monomer},$$

where a was empirically selected.

2.6. Dynamic light scattering measurements

2.6.1. Sample preparation

We performed non-seeded aggregation of 2.5 μM monomeric protein in aggregation buffer in a plate reader (24 repeats). Repeats that exhibited atypical kinetics of prefibrillar aggregates were transferred to an Eppendorf tube, mixed and used for measurements. Sample of fibrils was obtained by dilution of completely fibrillized 50 μM solution with 1× aggregation buffer to 2.5 μM concentration. Sample of monomeric protein was prepared by dilution of monomeric protein with 1× aggregation buffer to 2.5 μM concentration.

2.6.2. Measurements

The size distribution was measured using Zetasizer Nano ZS (Malvern Instruments) equipped with a 633 nm laser. Measurements were performed at 25 °C using quartz cuvettes. Each sample was measured 3 times (17 runs of 10 s). The density and refractive indexes were set to values recommended by device supplier for proteins in PBS buffer. The size distribution was calculated from raw cumulative curves using original software supplied with the device. Samples of monomeric protein and prefibrillar aggregates were monodisperse. In the case of

the sample containing fibrils, the fit did not pass quality criteria due to strong deviations at large-particle part of the distribution curve and the resulting average size was significantly different between the 3 measurements showing few peaks between 50 and 3000 nm. This polydispersity is due to the shape of fibrils (~1:1000 diameter to length ratio) that cannot be analyzed under the assumption of close to spherical shape of particles used for DLS analysis.

2.7. Testing seeding ability of prefibrillar aggregates

We performed non-seeded aggregation of 2.5 μM monomeric protein in aggregation buffer in a plate reader (24 repeats). Repeats that exhibited atypical kinetics of prefibrillar aggregates were transferred to an Eppendorf tube, mixed and used in the experiment. 2.5 μM fibrils were obtained by the dilution of a completely fibrillized 50 μM sample. Both prefibrillar aggregates and fibrils were diluted during the experiment by monomeric protein, yielding a final concentration of 1.25 μM.

We prepared samples containing 20 μM monomeric AS and 1.25 μM prefibrillar aggregates or fibrils. As a control we used 20 μM monomeric AS. We pipetted the obtained solutions to the plate (12 repeats for each sample) and measured fluorescence intensity as described above (section 2.2).

For all samples we measured aggregation lag time. It was determined as the time from the beginning of measurement to the time point where the growth switched to the exponential mode, i.e. the slope of the kinetic curve in the logarithmic scale increased by 30%. Samples containing 1.25 μM fibrils started to grow without any delay displaying typical curves of seeded aggregation, therefore lag time for them was taken as "0".

3. Results

3.1. Critical concentration of AS fibril growth is ~ 0.4 μM

In order to determine the critical concentration of AS fibril growth (the lowest concentration of monomeric AS capable of binding to the fibril end), we measured the rate of AS fibrillization at monomer concentrations ranging from 0.11 to 20 μM in the presence of small amount of short fibrils (seeds). Fibril growth was monitored using ThT, a fluorogenic dye that increases fluorescence upon binding to amyloid fibrils in a concentration-dependent manner **[3]** (Fig. S5 A, B). After the addition of seeds to AS solutions, we observed a rapid increase of ThT fluorescence in samples with AS concentration ≥ 0.45 μM and no fluorescence increase at concentrations ≤0.3 μM (Fig. 1A). Moreover, during the first hours we observed a slight decrease of fluorescence signal in samples with low AS concentration. We hypothesized that the decrease is caused by disaggregation of added seeds.

Binding of AS monomers to fibril ends is a reversible process. Therefore, the effective fibril growth rate is the difference between the rate of monomer binding to fibril end and the rate of its dissociation:

$$Rate = k_{binding} \times C_{ends} \times C_{monomer} - k_{dissociation} \times C_{ends};$$

$$Rate = k_{binding} \times C_{ends} \times (C_{monomer} - K_d).$$

If the monomer concentration is higher than K_d, fibrils elongate and if $C_{monomer} < K_d$, fibrils disaggregate. The concentration of fibril ends should impact the rate of the process but not the direction. We calculated K_d, or the constant of monomer dissociation from fibril ends, based on the relationship between the fibrillization rate and monomer concentration. Experimental data were fitted with a linear equation, yielding Kd as the intersection with x-axis (Fig. 1B). At this point rates of monomer association with fibril and its dissociation are equal, therefore monomer concentration is equal to K_d. Obtained K_d was 0.4 ± 0.05 μM.

To test if short AS fibrils dissociate to monomers at low concentrations, we monitored the stability of seeds (0.05–2 μM, here and further the concentrations of seeds and fibrils are presented as the concentration of protein molecules). We observed decreases in ThT fluorescence intensity for all samples (Fig. 1C) upon incubation during 24 h. The fraction of intact fibrils that remained after the incubation did not differ much for samples with a total AS concentration above 0.4 μM. However, the fraction of remaining fibrils significantly decreased in samples with a total AS concentration ≤ 0.4 μM, indicating disaggregation (Fig. 1D). We also observed disaggregation of samples obtained during seeded aggregation upon dilution below 0.4 μM total AS concentration (S-4, Fig. S6). The concentration at which seeds can completely disaggregate into monomers (≤0.4 μM) is very similar to the minimal concentration of AS monomer necessary for fibril elongation (~0.45 μM) which corresponds to the critical concentration of AS fibril growth and K_d value.

We also tested if the activity of seeds (ability to initiate fibril growth) changes after incubation. Namely, we added 20 μM monomeric AS to seeds incubated for 24 h and measured the fibril growth rate. Seeds of 0.05–0.2 μM concentrations, which is below the K_d, lost ~90% of seeding activity after incubation (Fig. 1E, F and S4), which points to almost complete disaggregation of seeds. On the contrary, seeds of 0.6–2 μM concentration (above the K_d) lost only ~25% of their activity after incubation (Fig. 1F and S4). The observed decrease in seeding activity correlates well with the decrease in the fraction of intact fibrils after 24 h incubation (Fig. 1D).

3.2. Three types of kinetic behaviour at different AS concentrations

The ThT fluorescence intensity in aggregating AS samples is proportional to the concentration of fibrillized protein (Fig. S5 A,B). Surprisingly, preliminary analysis of the final fluorescence intensity of samples presented in Fig. 1A revealed a non-linear increase of intensity with AS concentration (Fig. 2A and S5 C, D). Samples with low AS concentrations showed much lower fluorescence intensities than expected. This prompted us to analyze the kinetic curves in more detail.

At concentrations from 5 to 20 μM, AS rapidly fibrillized in the presence of 50 nM seeds exhibiting typical kinetics of AS seeded aggregation (Fig. 2A, green curves). At concentrations ≤0.3 μM, AS did not aggregate (red curves). To our surprise, samples of intermediate AS concentrations (0.45–3.75 μM) showed atypical fibril growth kinetics. ThT fluorescence increased to an identical level among these samples and then stabilized for a considerable period of time (Fig. 2A, blue curves, and Fig. S5 D). For a system where all AS is converted into the fibrillar form, the final fluorescence plateau value is proportional to the AS concentration and would have a higher intensity than the detected fluorescence signal. Therefore, we assumed that aggregates obtained in the samples with intermediate AS concentrations differ from fibrils. Moreover, samples that contain 5–20 μM AS exhibited typical growth kinetics, but at the beginning of experiment they had a sharp change in the fibrillization rate at the same fluorescence intensity as the „plateau "of atypical aggregation (Fig. 2A, green curves at 0–5 h). Similar atypical kinetics can be observed also in the absence of seeds, at early stages of AS aggregation at higher concentrations (Figs. 2B and S7). This implies that there is an intermediate state of AS that is formed faster than mature amyloid fibrils but is also able to bind ThT, which is a feature of amyloids.

The observed AS states (fibrils, intermediate amyloid aggregates and monomer) are stable at corresponding concentration ranges, as addition of new portions of seeds did not lead to any changes in the samples' state (Fig. S6 A, B). Dilution with buffer also had no effect on the most of samples (Fig. S6 C, D), with the exception of the samples of amyloid aggregates with the lowest concentration (0.45 and 0.6 μM AS). These samples showed a decrease in fluorescence intensity due to disaggregation upon dilution below the critical concentration (see section S-4 for more information).

The equilibrium between these three states slightly depends on the amount of added seeds (Fig. S9). Nevertheless, as all three states are observed also at non-seeded aggregation (Fig. S8), it is likely an

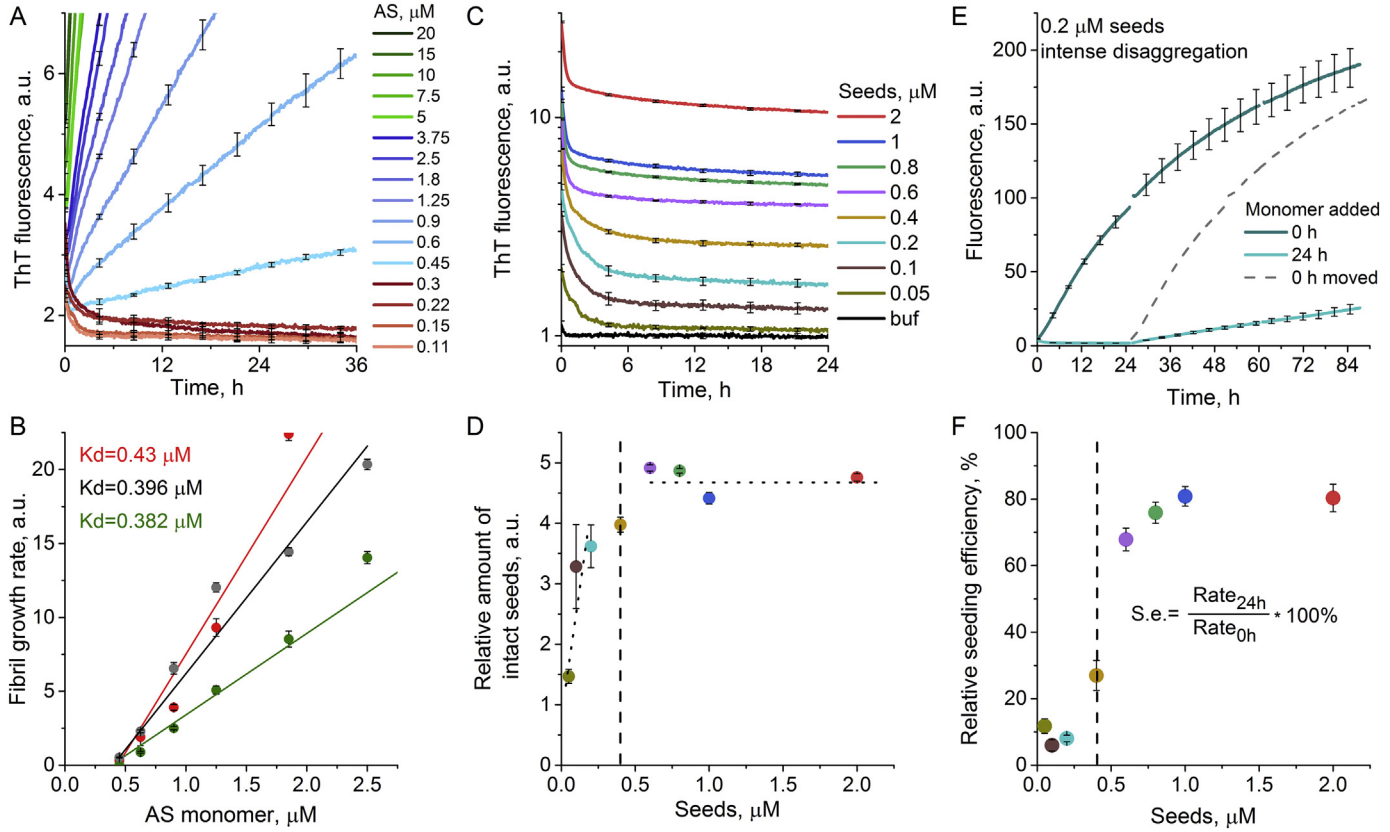

Fig. 1. A. Kinetic traces of AS aggregation in the presence of 50 nM seeds. 6 repeats per sample (n = 6). SD are shown for every 50th point. B. Fibril growth rates at low AS concentrations. Lines are fits to $rate = const(C_{monomer}\text{-}K_d)$. Data from 3 independent seeded aggregation experiments (in the presence of 50 nM seeds). Each point on graphs is an average of 6 samples. C. Kinetic traces of AS seeds disaggregation. n = 4. SD are shown for every 50th point. D. Relative amount of intact seeds, calculated as fluorescence intensity of seeds after 24 h of incubation normalized to the seeds concentration. n = 4. The vertical dashed line marks critical concentration of 0.4 μM. E. Kinetic traces of 20 μM AS aggregation in the presence of 0.2 μM seeds, mixed with monomer directly after the sonication (0 h) and after 24 h of seeds incubation. n = 4. SD are shown for every 50th point. Dashed curve represents "0 h" sample, copied and moved to the "24 h" sample for better comparison. F. Relative seeding efficiency of incubated seeds, calculated as a ratio of the fibril growth rate of samples where seeds were incubated for 24 h to the rate of the samples where seeds were mixed with the monomer directly, at 0 h (as shown e.g. in panel D), multiplied by 100%. n = 4. The vertical dashed line marks critical concentration of 0.4 μM.

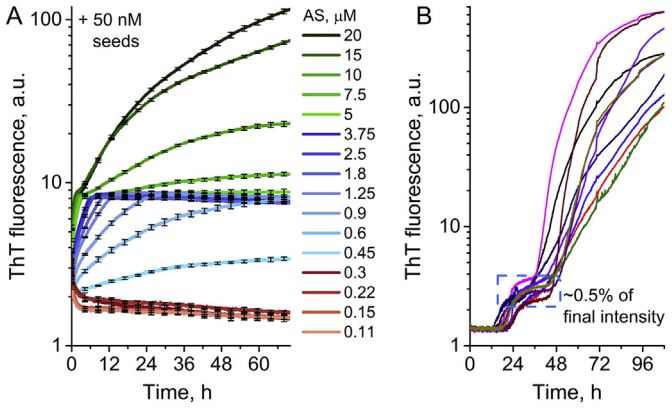

Fig. 2. A. Kinetic traces of AS aggregation in the presence of 50 nM seeds (the same experiment as shown in Fig. 1A). n = 6. SD are shown for every 50th point. Samples are divided into three groups: with typical growth (green), atypical growth (early amyloid aggregates, blue) and with no growth (red). B. Atypical kinetics of early amyloid aggregates (dashed rectangle) during non-seeded aggregation of 50 μM AS. 10 repeats.

intrinsic feature of AS aggregation.

3.3. Intermediate amyloid aggregates have similar structural properties but different morphology compared to typical fibrils

Although we observed atypical kinetics in samples of low micromolar concentration (0.45–3.75 μM), we could not be absolutely sure whether this kinetics was due to aggregates with the structure different from typical fibrils or whether some fibrillar species of different morphology (e.g. with a different periodicity or monofilamentous [21]) were detected. Therefore, we investigated the morphology of these aggregates using AFM imaging.

The samples that exhibited typical growth contained clearly visible fibrils with a height of ~8 nm (Fig. 3, samples 20, 10, 5 μM). The length of formed fibrils increased proportionally to AS concentration, from 0.5–1.5 μm at 5 μM AS to 2–6 μm at 20 μM AS. In the samples showing atypical aggregation kinetics (Fig. 3, samples 2.5 and 1.25 μM) we did not observe any fibrillar structures. These samples had very small round particle-like structures, ~4–8 nm in height, similar to previously described oligomers [12,25]. Samples with no growth (0.22 μM) contained thin layers of material (0.5–2 nm high) that most probably consists of monomeric protein.

The particles formed in samples with atypical aggregation kinetics have structure different from mature amyloid fibrils. We denoted these aggregates "prefibrillar amyloid aggregates", as their formation precedes the formation of mature fibrils and they are ThT positive, which is

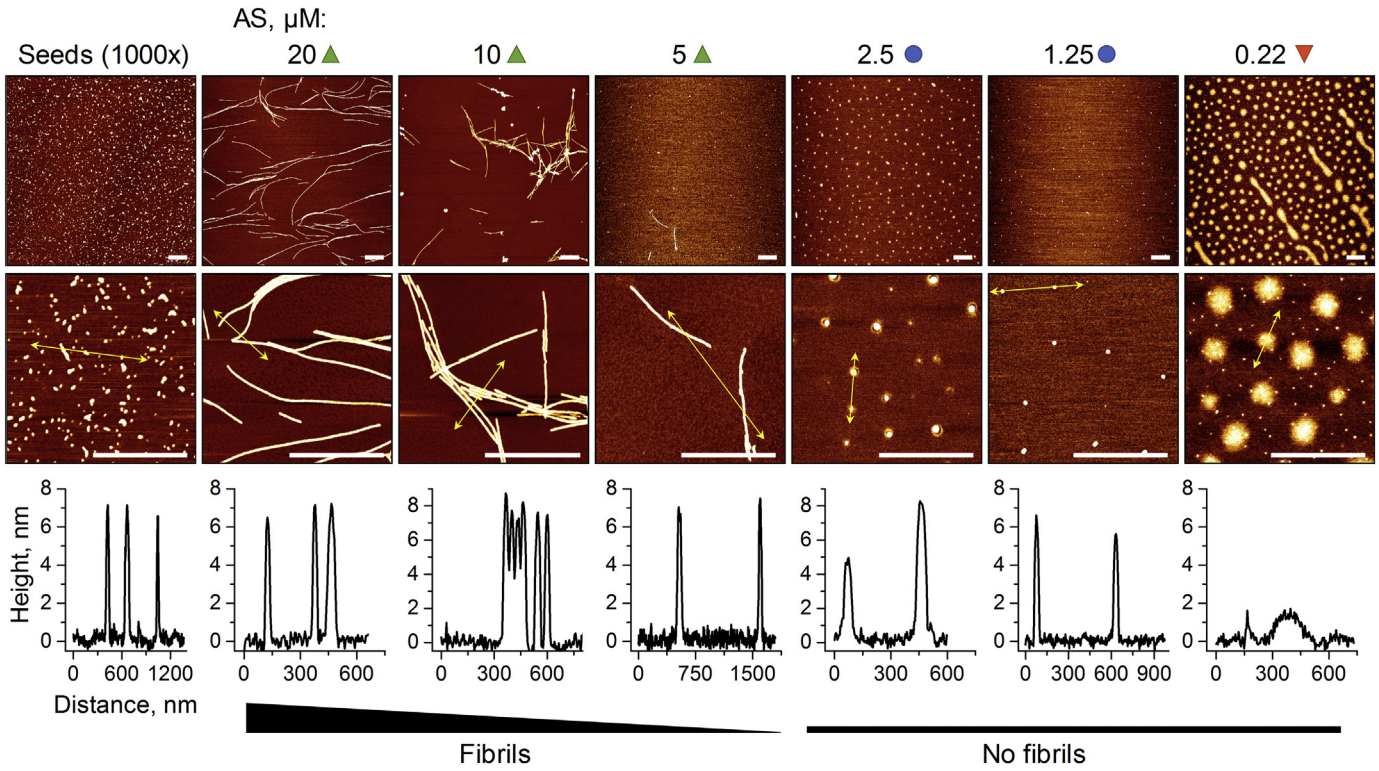

Fig. 3. Atomic force microscopy images of the seeds and AS aggregates formed after addition of the seeds (72 h of aggregation). Green triangles up represent fibrils (samples with typical growth), blue circles represent early amyloid aggregates (samples with atypical growth), red triangles down represent monomer (samples with no aggregation). White scale bar corresponds to 1 μm. Graphs on the lower panel represent the height profile of the fibrils measured at the sites marked with yellow arrows.

a feature of amyloids.

We performed dynamic light scattering (DLS) measurements to investigate whether in solution prefibrillar aggregates are of the same size as when dried on mica. The sample of 2.5 μM prefibrillar aggregates showed relatively narrow size distribution (Fig. 4A) with a hydrodynamic diameter of 20 ± 5 nm. Bigger size of prefibrillar aggregates in aqueous solution compared to dried on mica suggests that their structure is rather loose than compact. Under the same conditions monomeric protein showed structures about 3.8 nm in diameter. Fibrils showed multiple peaks ranging from 50 to 3000 nm because their very elongated shape cannot be properly approximated by a single hydrodynamic diameter and resulted distribution is too polydisperse.

The different morphology of prefibrillar amyloid aggregates compared to typical fibrils prompted us to study their intrinsic properties to obtain more information about protein structure. To investigate hydration and polarity of AS environment in studied aggregates, we used AS labelled with solvatochromic dyes XXL, 6FM, 7AFM and FPM. These dyes change emission spectra depending on their environment and were shown to distinguish different states of AS [23]. We introduced fluorescent probes into aggregates by co-aggregation of 50, 20 and 2 μM AS with 400 nM labelled AS cysteine mutant. (Figs. 4B,C and S11). All samples showed an increase in the fluorescence intensity and a shift of the emission band after 42 h incubation, confirming the aggregation of AS (Figs. 4B, C and S11). Spectra of early amyloid aggregates (2 μM) exhibited the same features as those of fibrils (50 and 20 μM) and differed from spectra of monomeric protein. For instance, spectra of dyes XXL (Fig. 4B, C) and 6FM (Fig. S11C, D) exhibited a blue shift of the emission peak. The spectrum of 7AFM dye in prefibrillar amyloid aggregates exhibited changes in the emission bands ratio typical for fibrillized AS [23] (Fig. S11 E, F). Four different environmentally sensitive probes reported similarity of AS environment polarity and hydration between the prefibrillar amyloid aggregates and fibrils. We, therefore, concluded that AS in the aggregates is tightly packed and is likely in a β-sheet rich form similar to its form in fibrils.

We compared β-sheet content in fibrils and prefibrillar amyloid aggregates using CD spectroscopy (Fig. 4D). The peak in CD spectra that corresponds to β-sheet content was significantly higher in sample with 2.5 μM prefibrillar amyloid aggregates than the combination of signals of monomeric protein and seeds used for aggregation initiation (50 nM). The signal of prefibrillar amyloid aggregates was lower than the signal of fibrils, though. High β-sheet content of prefibrillar aggregates proves their amyloid nature and clearly indicates that prefibrillar amyloid aggregates are structurally closer to fibrils than to monomers.

3.4. *Prefibrillar amyloid aggregates can seed AS fibril growth, although less efficiently than fibrils*

The observed aggregates can be either intermediates of AS fibrillization or so-called 'off-pathway' oligomers that do not participate in further fibrillization. The 'on-pathway' and 'off-pathway' species can be distinguished by ability or disability to accelerate AS fibril formation. To test if the studied prefibrillar aggregates are able to accelerate AS fibrillization we mixed them with monomeric AS and monitored fibril formation (Fig. 5A).

Addition of 1.25 μM prefibrillar aggregates to monomeric protein accelerated aggregation of monomeric AS. Namely, it led to ~2.4-fold decrease in average lag time compared to lag time of 20 μM monomer alone (Fig. 5B). Therefore, we conclude that prefibrillar amyloid aggregates can seed AS fibril formation, although no fibril-like structures are observed in the prefibrillar amyloid aggregates sample before monomer addition (Fig. 5C, D). Nevertheless, the seeding efficiency of prefibrillar amyloid aggregates was much lower than that of fibrils of the same concentration (Fig. 5A, B).

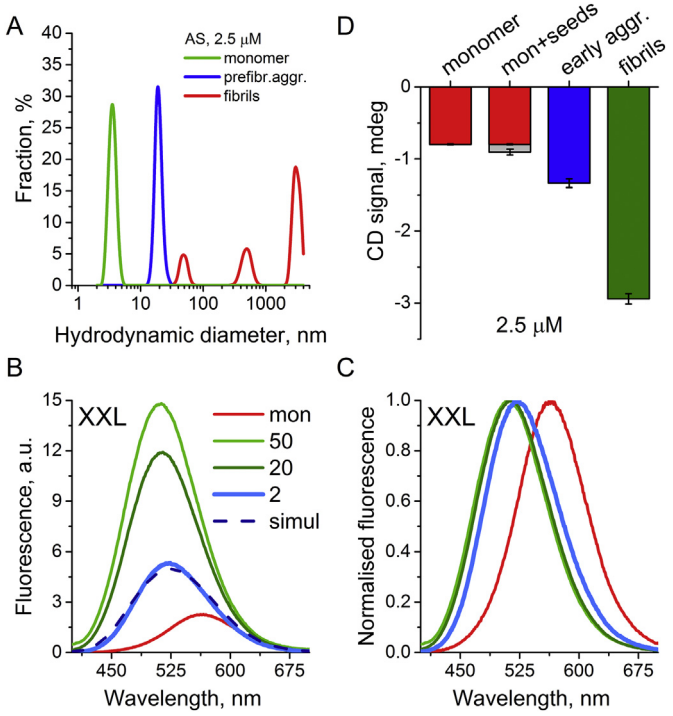

Fig. 4. Characterization of aggregated samples. A. Size distribution of monomeric AS, prefibrillar aggregates and fibrils according to DLS measurements (volume fractions). AS concentration was 2.5 μM in each sample. For the raw correlation curves see Fig. S10. B, C. Sensing AS aggregation using environmentally sensitive XXL dye. B. Emission spectra of monomeric 400 nM XXL-labelled AS, and aggregation solution of 2, 20 and 50 μM AS in the presence of 400 nM XXL-labelled AS and 200 nM seeds, and simulated spectrum of a solution that contains 35% fibrillized and 65% monomeric protein. C. Normalized fluorescence spectra from the panel B. D. CD-signal of 2.5 μM AS in monomeric state, state of prefibrillar amyloid aggregates (48 h of aggregation) and fibrillar state; and combined CD-signal of 2.5 μM monomer and 50 nM seeds used for initiation of aggregation. Values were obtained as average signal from 217 to 220 nm. $n = 3$.

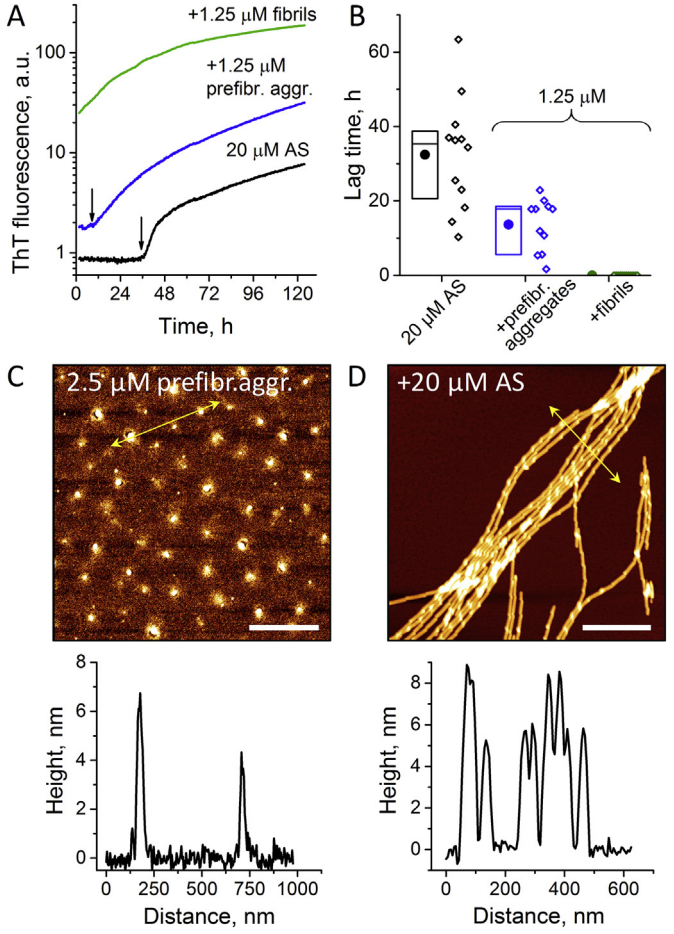

Fig. 5. A. Fibrillization of 20 μM AS without seeds (black), in the presence of 1.25 μM prefibrillar amyloid aggregates (blue) or fibrils (green). Black arrows mark lag times. B. Lag times of 20 μM AS when non-seeded and seeded by 1.25 μM prefibrillar amyloid aggregates samples and by the fibrils. C, D. AFM images of the (C) prefibrillar amyloid aggregate sample (2.5 μM) and (D) the fibrils formed after mixing the sample with 20 μM AS. White scale bar corresponds to 0.5 μm. Graphs on the lower panel represent height profiles measured at the sites marked with yellow arrows.

4. Discussion

AS aggregation is involved in the pathophysiology of Parkinson's disease. To develop inhibitors specific to the early steps of aggregation, it is important to better understand the nature of the intermediate species in monomer conversion to fibrils; to determine the concentration at which fibrils start to form and to grow, and whether already formed fibrils can disaggregate. To tackle these questions, we studied the kinetics of both seeded and non-seeded aggregation of AS at low concentrations and characterized the obtained aggregates.

Measurements of fibril growth and disaggregation at different AS concentrations (Figs. 1A, 2A and S6) show that monomeric AS at concentrations ≥0.45 μM is able to bind to short fibrils (seeds). At lower concentrations, though, fibrils disaggregate. Binding of monomeric AS to fibril ends and its dissociation are reversible processes. The rate of monomer dissociation depends only on the concentration of fibril ends, while the rate of monomer binding increases with monomer concentration. The interplay of these two reactions determines the behaviour of AS in solution. Above the critical concentration monomer binding to fibril ends dominates over dissociation, while below the critical concentration dissociation of monomers dominates over binding. Therefore, at low concentrations fibrils disaggregate until monomer concentration reaches K_d values or all fibrils disappear. Consequently, the presence of monomer in solution slows down fibril disaggregation if $C_{monomer} < K_d$ (Fig. S12); when $C_{monomer} > K_d$, fibrils do not disaggregate but grow. The affinity constant of monomeric AS to fibril ends (K_d) is ≈0.4 μM and is equal to the critical concentration of AS fibril growth. This value corresponds to the free energy of fibril elongation of approx. 36.5 kJ/mol that agrees well with thermodynamic stability of AS fibril determined by denaturation experiments (ΔG = 33 ± 2 kJ/mol) [26].

Our data correlate well with a report showing degradation of 0.07 μM AS non-sonicated fibrils and of 0.07–17.5 μM AS fibrils upon continuous ultrasonication [18]. Moreover, similar behaviour was observed for another amyloid protein Aβ (1–40). Its critical concentration was shown to be 0.7–1 μM, which corresponds to the K_d of Aβ (1–40) fibrils [27,28]. Aβ (1–40) fibrils disaggregated below the critical concentration upon ultrasonication [28].

Fibril growth and initial fibril formation are different processes and therefore may require different minimal AS concentrations to start. We observed fibril formation in the absence of seeds at concentrations as low as 10 μM (Fig. S8). This correlates well with the reports of other research groups claiming critical concentration of fibril formation to be at ≈15 μM [15]. Interestingly, this value is higher than the critical concentration of fibril growth. Indeed, our experiments show that at monomer concentrations between 0.4 and 10 μM new fibrils do not form (Fig. S8), but already formed fibrils can grow (Fig. 2A). Therefore, we assume that fibrils, which have already appeared at higher concentrations, will grow even if AS concentration drops below 10 μM.

Table 1
Comparison of different AS states.

Feature	Monomers	Prefibrillar amyloid aggregates	Fibrils
ThT fluorescence	−	+/− Not proportional to AS concentration	+ Proportional to AS concentration
Can seed fibril formation/growth	−	+/− Less efficient than fibrils	+
β-sheet conformation (according to CD spectroscopy)	−	+	+
Fibrils visible by AFM	−	−	+
Size	~3.8 nm (DLS data)	~4–8 nm (AFM data) ~20 nm (DLS data)	~2.6 μm × 8 nm (AFM data) ~50–3000 nm (DLS data)
Stability upon dilution	+	Disaggregates upon dilution below the critical concentration, otherwise stable	Disaggregates upon dilution below the critical concentration, otherwise stable

These fibrils will disaggregate only when AS concentration drops below 0.4 μM.

Depending on AS concentration, we observed three different kinetic behaviours: i) the typical growth kinetics of fibrils; ii) the total absence of growth of monomeric protein below the critical concentration; and iii) the atypical kinetics of the prefibrillar amyloid aggregates (Figs. 2A, S6 and S9). This atypical kinetics was also detected at early stages of non-seeded aggregation at much higher AS concentrations (50–100 μM, Figs. 2B and S7). We hypothesized that prefibrillar amyloid aggregates are intermediate species between monomers and fibrils and exhibit this atypical kinetics.

Prefibrillar amyloid aggregates have properties similar to both monomeric and fibrillar states of AS, although they are closer to fibrils (Table 1). For instance, prefibrillar amyloid aggregates have higher β-sheet content than monomeric protein, although lower than fibrils (Fig. 4D). The spectra of environmentally sensitive dyes in prefibrillar amyloid aggregates are similar to the spectra in fibrils (Figs. 4B, C and S11). Moreover, unlike monomers, prefibrillar amyloid aggregates can seed fibril growth (Figs. 5 and S12). Nevertheless, prefibrillar amyloid aggregates have a different morphology than fibrils. Early aggregates appear to be roundish particles of loose structure, ~4–8 nm high in dry state (according to AFM, Figs. 3 and 5C) and ~20 nm in diameter when in solution (according to DLS, Fig.4A).

Some of the earlier described oligomers had features (β-sheet structure, seeding capability) [8] similar to those of prefibrillar amyloid aggregates described here. However, the atypical kinetics of prefibrillar amyloid aggregates has not been described yet to the best of our knowledge. We assume that prefibrillar amyloid aggregates might be one of the species in a very diverse group of AS oligomers, although we prefer the term “prefibrillar amyloid aggregates” as it better describes their properties.

As described prefibrillar amyloid aggregates are able to seed fibrillization of AS; they are structurally much closer to fibrils than relatively stable AS oligomers that are formed in concentrated solutions and were reported to inhibit the fibril growth [25] or not to convert to fibrils upon long incubation in the presence of excess of monomeric protein [29,30].

Our data are in line with the observation of oligomer formation at low micromolar concentrations (0.5–2.5 μM) [11], with the detection of aggregates that were several nanometers in size in 5 and 10 μM AS solutions [15], as well as with the observation of β-sheet-specific CD-signal at the early stages of AS aggregation, when no fibrils are seen by means of AFM [31].

Prefibrillar amyloid aggregates can interconvert to both monomeric and fibrillar states of AS (Fig. 6). Prefibrillar aggregates are formed in the concentration range 0.45–3 μM during the aggregation process and can disaggregate to monomer upon decrease in protein concentration. Meanwhile, conversion of prefibrillar amyloid aggregates to fibrils is irreversible, since disaggregation of fibrils leads to monomeric protein only.

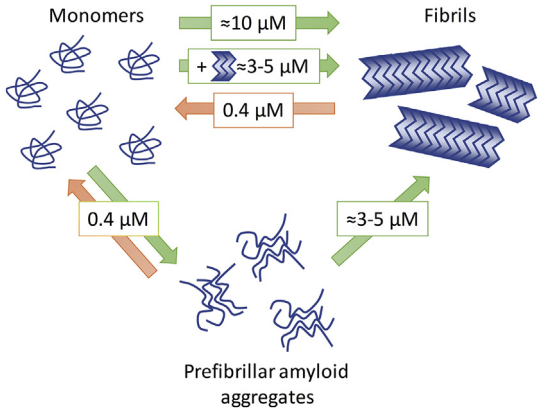

Fig. 6. Interconnection between different states of AS – monomers, prefibrillar amyloid aggregates and fibrils.

5. Conclusions

We investigated aggregation of AS at low concentrations. For the first time to our knowledge, we determined the critical concentration of fibril growth separately from the critical concentration of fibril formation. Namely, we showed that fibrils can recruit monomeric AS resulting in fibril elongation at concentrations of monomeric AS in the solution as low as 0.4 ± 0.05 μM. This concentration is significantly lower than the AS concentration required for de novo fibril formation (≈10 μM). Furthermore, we demonstrated that below the critical concentration of fibril growth, fibril disaggregation dominates over fibril growth. We found that AS of concentrations 0.4–3.5 μM, which is between two critical concentrations, has atypical kinetics of aggregation and forms stable prefibrillar amyloid aggregates. These aggregates can induce fibril growth and therefore may be intermediate species that appear during monomer conversion to fibrils at higher AS concentrations.

Acknowledgements

Dr. Valery Andrushchenko and Dr. Lucie Bednárová are acknowledged for providing support with CD measurements.

Funding

This work was supported by IOCB installation grant and the Czech Science Foundation [GACR grant 18-06255Y]. The AFM setup was supported by VaVpI [CZ.1.05/4.1.00/16.0340] and UNCE/SCI/010.

Conflict of interest

The authors declare that they have no conflicts of interest with the

contents of this article.

Appendix A. Supplementary data

Supplementary data to this article can be found online at https://doi.org/10.1016/j.bbapap.2019.05.003.

References

[1] J.C. Bridi, F. Hirth, Mechanisms of α-Synuclein induced Synaptopathy in Parkinson's disease, Front. Neurosci. 12 (2018) 80.
[2] D. Snead, D. Eliezer, α-Synuclein function and dysfunction on cellular membranes, Exp Neurobiol 23 (2014) 292–313.
[3] V.V. Shvadchak, M.M. Claessens, V. Subramaniam, Fibril breaking accelerates α-synuclein fibrillization, J. Phys. Chem. B 119 (2015) 1912–1918.
[4] R. Kumar, S. Das, G.M. Mohite, S.K. Rout, S. Halder, N.N. Jha, S. Ray, S. Mehra, V. Agarwal, S.K. Maji, Cytotoxic oligomers and fibrils trapped in a gel-like state of α-synuclein assemblies, Angew. Chem. Int. Ed. Eng. 57 (2018) 5262–5266.
[5] M.L. Choi, S. Gandhi, Crucial role of protein oligomerization in the pathogenesis of Alzheimer's and Parkinson's diseases, FEBS J. 285 (2018) 3631–3644.
[6] J.A. Fauerbach, D.A. Yushchenko, S.H. Shahmoradian, W. Chiu, T.M. Jovin, E.A. Jares-Erijman, Supramolecular non-amyloid intermediates in the early stages of α-synuclein aggregation, Biophys. J. 102 (2012) 1127–1136.
[7] W. Paslawski, M. Andreasen, S.B. Nielsen, N. Lorenzen, K. Thomsen, J.D. Kaspersen, J.S. Pedersen, D.E. Otzen, High stability and cooperative unfolding of α-synuclein oligomers, Biochemistry 53 (2014) 6252–6263.
[8] N. Cremades, S.W. Chen, C.M. Dobson, Structural characteristics of α-Synuclein oligomers, Int. Rev. Cell Mol. Biol. 329 (2017) 79–143.
[9] B. Winner, R. Jappelli, S.K. Maji, P.A. Desplats, L. Boyer, S. Aigner, C. Hetzer, T. Loher, M. Vilar, S. Campioni, C. Tzitzilonis, A. Soragni, S. Jessberger, H. Mira, A. Consiglio, E. Pham, E. Masliah, F.H. Gage, R. Riek, In vivo demonstration that α-synuclein oligomers are toxic, Proc. Natl. Acad. Sci. U. S. A. 108 (2011) 4194–4199.
[10] N. Plotegher, E. Gratton, L. Bubacco, Number and brightness analysis of α-synuclein oligomerization and the associated mitochondrial morphology alterations in live cells, Biochim. Biophys. Acta 1840 (2014) 2014–2024.
[11] M. Iljina, A.J. Dear, G.A. Garcia, S. De, L. Tosatto, P. Flagmeier, D.R. Whiten, T.C.T. Michaels, D. Frenkel, C.M. Dobson, T.P.J. Knowles, D. Klenerman, Quantifying co-oligomer formation by α-Synuclein, ACS Nano 12 (2018) 10855–10866.
[12] G. Fusco, S.W. Chen, P.T.F. Williamson, R. Cascella, M. Perni, J.A. Jarvis, C. Cecchi, M. Vendruscolo, F. Chiti, N. Cremades, L. Ying, C.M. Dobson, A. De Simone, Structural basis of membrane disruption and cellular toxicity by α-synuclein oligomers, Science 358 (2017) 1440–1443.
[13] B.G. Wilhelm, S. Mandad, S. Truckenbrodt, K. Krohnert, C. Schafer, B. Rammner, S.J. Koo, G.A. Classen, M. Krauss, V. Haucke, H. Urlaub, S.O. Rizzoli, Composition of isolated synaptic boutons reveals the amounts of vesicle trafficking proteins, Science 344 (2014) 1023–1028.
[14] S.J. Wood, J. Wypych, S. Steavenson, J.C. Louis, M. Citron, A.L. Biere, Aα-Synuclein fibrillogenesis is nucleation-dependent. Implications for the pathogenesis of Parkinson's disease, J. Biol. Chem. 274 (1999) 19509–19512.
[15] M.E. van Raaij, J. van Gestel, I.M. Segers-Nolten, S.W. de Leeuw, V. Subramaniam, Concentration dependence of α-synuclein fibril length assessed by quantitative atomic force microscopy and statistical-mechanical theory, Biophys. J. 95 (2008) 4871–4878.
[16] M. Necula, C.N. Chirita, J. Kuret, Rapid anionic micelle-mediated α-synuclein fibrillization in vitro, J. Biol. Chem. 278 (2003) 46674–46680.
[17] A.P. Pandey, F. Haque, J.C. Rochet, J.S. Hovis, Clustering of α-synuclein on supported lipid bilayers: role of anionic lipid, protein, and divalent ion concentration, Biophys. J. 96 (2009) 540–551.
[18] H. Yagi, A. Mizuno, M. So, M. Hirano, M. Adachi, Y. Akazawa-Ogawa, Y. Hagihara, T. Ikenoue, Y.H. Lee, Y. Kawata, Y. Goto, Ultrasonication-dependent formation and degradation of α-synuclein amyloid fibrils, Biochim. Biophys. Acta 1854 (2015) 209–217.
[19] S. Banerjee, M. Hashemi, Z. Lv, S. Maity, J.C. Rochet, Y.L. Lyubchenko, A novel pathway for amyloids self-assembly in aggregates at nanomolar concentration mediated by the interaction with surfaces, Sci. Rep. 7 (2017) 45592.
[20] M. Rabe, A. Soragni, N.P. Reynolds, D. Verdes, E. Liverani, R. Riek, S. Seeger, On-surface aggregation of α-synuclein at nanomolar concentrations results in two distinct growth mechanisms, ACS Chem. Neurosci. 4 (2013) 408–417.
[21] J.W.P. Brown, G. Meisl, T.P.J. Knowles, A.K. Buell, C.M. Dobson, C. Galvagnion, Kinetic barriers to α-synuclein protofilament formation and conversion into mature fibrils, Chem. Commun. (Camb.) 54 (2018) 7854–7857.
[22] K. Afitska, A. Fucikova, V.V. Shvadchak, D.A. Yushchenko, Modification of C terminus provides new insights into the mechanism of α-Synuclein aggregation, Biophys. J. 113 (2017) 2182–2191.
[23] O.A. Kucherak, V.V. Shvadchak, Y.A. Kyriukha, D.A. Yushchenko, Synthesis of a fluorescent probe for sensing multiple protein states, Eur. J. Org. Chem. (2018) 5155–5162.
[24] V.V. Shvadchak, O. Kucherak, K. Afitska, D. Dziuba, D.A. Yushchenko, Environmentally sensitive probes for monitoring protein-membrane interactions at nanomolar concentrations, Biochim. Biophys. Acta Biomembr. 1859 (2017) 852–859.
[25] N. Lorenzen, S.B. Nielsen, A.K. Buell, J.D. Kaspersen, P. Arosio, B.S. Vad, W. Paslawski, G. Christiansen, Z. Valnickova-Hansen, M. Andreasen, J.J. Enghild, J.S. Pedersen, C.M. Dobson, T.P. Knowles, D.E. Otzen, The role of stable α-synuclein oligomers in the molecular events underlying amyloid formation, J. Am. Chem. Soc. 136 (2014) 3859–3868.
[26] A.J. Baldwin, T.P. Knowles, G.G. Tartaglia, A.W. Fitzpatrick, G.L. Devlin, S.L. Shammas, C.A. Waudby, M.F. Mossuto, S. Meehan, S.L. Gras, J. Christodoulou, S.J. Anthony-Cahill, P.D. Barker, M. Vendruscolo, C.M. Dobson, Metastability of native proteins and the phenomenon of amyloid formation, J. Am. Chem. Soc. 133 (2011) 14160–14163.
[27] B. O'Nuallain, S. Shivaprasad, I. Kheterpal, R. Wetzel, Thermodynamics of a beta(1-40) amyloid fibril elongation, Biochemistry 44 (2005) 12709–12718.
[28] H. Yagi, K. Hasegawa, Y. Yoshimura, Y. Goto, Acceleration of the depolymerization of amyloid beta fibrils by ultrasonication, Biochim. Biophys. Acta 1834 (2013) 2480–2485.
[29] N. Cremades, S.I. Cohen, E. Deas, A.Y. Abramov, A.Y. Chen, A. Orte, M. Sandal, R.W. Clarke, P. Dunne, F.A. Aprile, C.W. Bertoncini, N.W. Wood, T.P. Knowles, C.M. Dobson, D. Klenerman, Direct observation of the interconversion of normal and toxic forms of α-synuclein, Cell 149 (2012) 1048–1059.
[30] N. Zijlstra, C. Blum, I.M. Segers-Nolten, M.M. Claessens, V. Subramaniam, Molecular composition of sub-stoichiometrically labeled α-synuclein oligomers determined by single-molecule photobleaching, Angew. Chem. Int. Ed. Eng. 51 (2012) 8821–8824.
[31] F.S. Ruggeri, J. Adamcik, J.S. Jeong, H.A. Lashuel, R. Mezzenga, G. Dietler, Influence of the beta-sheet content on the mechanical properties of aggregates during amyloid fibrillization, Angew. Chem. Int. Ed. Eng. 54 (2015) 2462–2466.